Quaternary Science Reviews 225 (2019) 105990

Contents lists available at ScienceDirect

Quaternary Science Reviews

journal homepage: www.elsevier.com/locate/quascirev

A new mechanism for millennial scale positive precipitation anomalies over tropical South America

Marília C. Campos [a, *], Cristiano M. Chiessi [a], Matthias Prange [b], Stefan Mulitza [b], Henning Kuhnert [b], André Paul [b], Igor M. Venancio [c], Ana Luiza S. Albuquerque [d], Francisco W. Cruz [e], André Bahr [f]

[a] School of Arts, Sciences and Humanities, University of São Paulo, São Paulo, Brazil
[b] MARUM – Center for Marine Environmental Sciences, University of Bremen, Bremen, Germany
[c] Center for Weather Forecasting and Climate Studies (CPTEC), National Institute for Space Research (INPE), Cachoeira Paulista, Brazil
[d] Graduate Program in Geochemistry, Fluminense Federal University, Niterói, Brazil
[e] Institute of Geociences, University of São Paulo, São Paulo, Brazil
[f] Institute of Earth Sciences, Heidelberg University, Heidelberg, Germany

ARTICLE INFO

Article history:
Received 21 August 2019
Received in revised form
3 October 2019
Accepted 3 October 2019
Available online 11 October 2019

Keywords:
Quaternary
Paleoclimatology
South America
Inorganic geochemistry
Heinrich Stadials
Precipitation
X-ray fluorescence

ABSTRACT

Continental and marine paleoclimate archives from northwestern and northeastern South America recorded positive precipitation anomalies during Heinrich Stadials (HS). These anomalies have been classically attributed to enhanced austral summer (monsoon) precipitation. However, the lack of marine paleoclimate records off eastern South America as well as inconsistencies between southeastern South American continental and marine records hamper a comprehensive understanding of the mechanism responsible for (sub-) tropical South American hydroclimate response to HS. Here we investigate piston core M125-95-3 collected off eastern South America (10.94°S) and simulate South American HS conditions with a high-resolution version of an atmosphere-ocean general circulation model. Further, meridional changes in precipitation over (sub-) tropical South America were assessed with a thorough compilation of previously available marine paleorecords. Our ln(Ti/Ca) and ln(Fe/K) data show increases during HS6-Younger Dryas. It is the first core off eastern South America and the southernmost from the Atlantic continental margin of South America that unequivocally records HS-related positive precipitation anomalies. Based on our new data, model results and the compilation of available marine records, we propose a new mechanism for the positive precipitation anomalies over tropical South America during HS. The new mechanism involves austral summer precipitation increases only over eastern South America while the rest of tropical South America experienced precipitation increases during the winter, challenging the widely held assumption of a strengthened monsoon. South American precipitation changes were triggered by dynamic and thermodynamic processes including a stronger moisture supply from the equatorial North Atlantic (tropical South Atlantic) in austral winter (summer).

1. Introduction

Reductions in the Atlantic meridional overturning circulation (AMOC) cross-equatorial heat transport associated with Heinrich Stadials (HS) affected South American hydroclimate (Arz et al., 1998; Kageyama et al., 2013). The mechanism usually invoked to explain HS precipitation anomalies over South America includes an enhanced South American monsoon system (SAMS), a southward migration of the Intertropical Convergence Zone (ITCZ) and an intensification of the South Atlantic Convergence Zone (SACZ) (Kanner et al., 2012; Peterson et al., 2000; Stríkis et al., 2015).

Continental paleoclimate records from northern (N) South America (e.g. Zular et al., 2019) show negative precipitation anomalies during HS that are supported by model simulations (Kageyama et al., 2013; Mohtadi et al., 2016). Positive precipitation anomalies over northwestern (NW) (e.g. Baker et al., 2001; Kanner et al., 2012), northeastern (NE) (e.g. Cruz et al., 2009; Ledru et al., 2006), and eastern (E) (e.g. Stríkis et al., 2018; Wang et al., 2004)

* Corresponding author.
E-mail address: marilia.carvalho.campos@usp.br (M.C. Campos).

https://doi.org/10.1016/j.quascirev.2019.105990
0277-3791/

South America during HS are equally supported by model results (Kageyama et al., 2013; Mohtadi et al., 2016). On the other hand, some continental paleoclimate records from southeastern (SE) South America (Cruz et al., 2007; Wang et al., 2006) suggest positive precipitation anomalies during HS, but are not supported by model simulations, which suggest no or even negative changes in precipitation (Kageyama et al., 2013; Mohtadi et al., 2016).

Marine paleoclimate records from the Atlantic continental margin of South America agree with model simulations and suggest negative precipitation anomalies over N South America (e.g. Bahr et al., 2018; Deplazes et al., 2013), positive precipitation anomalies over NW (e.g. Crivellari et al., 2018; Zhang et al., 2017) and NE (e.g. Arz et al., 1998; Mulitza et al., 2017) South America and no major changes in precipitation over SE South America (e.g. Behling et al., 2002; Gu et al., 2017) during HS. So far, no marine paleoclimate record covering the late Quaternary is available between ca. 7°S and 20°S off E South America.

The inconsistency between continental and marine paleoclimate records from SE South America together with the lack of marine records off E South America hamper the validation of the proposed mechanism behind (sub-) tropical South American hydroclimate response to HS.

Here we reduce the gap of marine paleoclimate records between 7°S and 20°S by investigating piston core M125-95-3 collected at 10.94°S (Fig. 1a). Our core site is influenced by the terrigenous discharge of the São Francisco River and recorded the hydroclimate history of E South America for the last ca. 70 ka. To reconstruct changes in precipitation over the São Francisco River drainage basin we determined the major elemental intensity along the piston core. In order to investigate meridional changes in precipitation over (sub-) tropical South America we performed a thorough compilation of available marine paleoclimate records. To scrutinize the mechanism responsible for hydroclimate changes, we performed a HS simulation with a high-resolution version of the atmosphere-ocean general circulation model CCSM3 (Collins et al., 2006).

Based on the combination of data from our core, the compilation of marine paleoclimate records and the model results we propose a new mechanism responsible for the last glacial HS positive precipitation anomalies over tropical South America to the south of the equator. The new mechanism involves dynamic and thermodynamic processes and shows an austral winter (summer) equatorial North Atlantic (tropical South Atlantic) moisture flux contributing to wetter conditions over NW South America (E South America) during HS.

2. Regional setting

During austral summer (winter), the main source of moisture for tropical South America is the North Atlantic (South Atlantic) via prevailing NE trade winds (SE trade winds). The austral summer NE trade winds moisture transport allows the development of the SAMS, whose convective rains are responsible for more than 50% of the total annual precipitation over tropical South America to the east of the Andes (Zhou and Lau, 1998). The onset of the SAMS occurs during austral spring (October), reaching its mature phase during the austral summer (December–February) with intense convection over the southern Amazon basin, and demising during austral fall (April) (Marengo et al., 2001).

The ITCZ and the SACZ are important phenomena in South American hydroclimate, both related to the SAMS. The ITCZ can be understood as a global convective belt over the oceans associated to the ascending branch of the Hadley cell and to the convergence of the NE and SE trade winds. In order to compensate the AMOC's northward cross-equatorial heat transport, the ITCZ mean latitudinal position is around 5°N (Marshall et al., 2014). The ITCZ shifts seasonally towards the summer hemisphere, following the highest sea surface temperatures (SST) (Schneider et al., 2014). It is believed that the southward migration of the ITCZ can induce periods of enhanced SAMS (Vuille et al., 2012). The SACZ can be understood as a NW-SE elongated convective belt that typically originates in the western Amazon basin in early August and extends southeastwards above SE South America, frequently reaching the adjacent western South Atlantic (Carvalho et al., 2004). During intense (weak) phases and, thus, enhanced (reduced) SAMS, the SACZ is displaced northwards (southwards) promoting a decrease in precipitation over SE South America south (north) of ca. 25°S (Robertson and Mechoso, 2000).

Despite the SAMS/SACZ influence, SE South America shows no marked seasonality, and year-round precipitation has two distinct sources: while the SAMS is the source for austral summer/early autumn precipitation, the extratropical South Atlantic is the precipitation source for the winter/early spring (Zhou and Lau, 1998).

Northern Hemisphere SST anomalies also play a fundamental role in South American hydroclimate by influencing the strength of the SAMS, where negative (positive) SST anomalies are related to a strong (weak) SAMS (Talento and Barreiro, 2017). In addition, positive SST anomalies in the western South Atlantic have been correlated to increased SACZ precipitation (Chaves and Nobre, 2004).

The São Francisco River drainage basin is the source of terrigenous sediments to our core site. It is the largest drainage basin in E South America (Fig. 1a). Most of the drainage basin shows a semi-arid climate but its headlands show humid conditions due to the influence of the SACZ, where most of the precipitation occurs during the austral summer. Its annual-mean water discharge is around 2980 m^3/s (Dominguez, 1996). Additionally, other five South American drainage basins are depicted in Fig. 1a and will be discussed herein. They are the Amazon (ca. 200000 m^3/s; Lentz, 1995), Parnaíba (ca. 640 m^3/s; Knoppers et al., 1999), Doce (ca. 624.4 m^3/s; Oliveira and Quaresma, 2017), Itajaí (ca. 230 m^3/s; Schettini, 2002) and La Plata (ca. 21000 m^3/s; Berbery and Barros, 2002) River drainage basins.

The marine records compiled herein were collected from the Atlantic continental margin off South America. At this portion of the western Atlantic, the upper water column (down to ca. 500 m water depth) is influenced by the northward flowing North Brazil Current and southward flowing Brazil Current, both originating at 10–14°S (Peterson and Stramma, 1991; Stramma and England, 1999). Between ca. 500 and 1200 m water depth, the western Atlantic is dominated by a northward and a southward flowing branch of the Intermediate Western Boundary Current originating at ca. 25°S (Stramma and England, 1999). The Deep Western Boundary Current flows southwards between ca. 1200 and 4000 m water depth (Stramma and England, 1999). It is noteworthy that the southwestern South Atlantic presents regions of strong bottom current activity (e.g. Faugères and Stow, 1993) that could bias the climatic signal of the SE South American cores compiled here (Behling et al., 2002; Campos et al., 2019; Gu et al., 2017). However, contouritic deposits in this region (Duarte and Viana, 2007) are only present at deeper water depths and hence do not affect the compiled marine cores.

3. Material and methods

3.1. Marine sediment core

We investigated piston core M125-95-3 (10.94°S, 36.20°W, 1897 m water depth, 10.4 m core length) collected from the

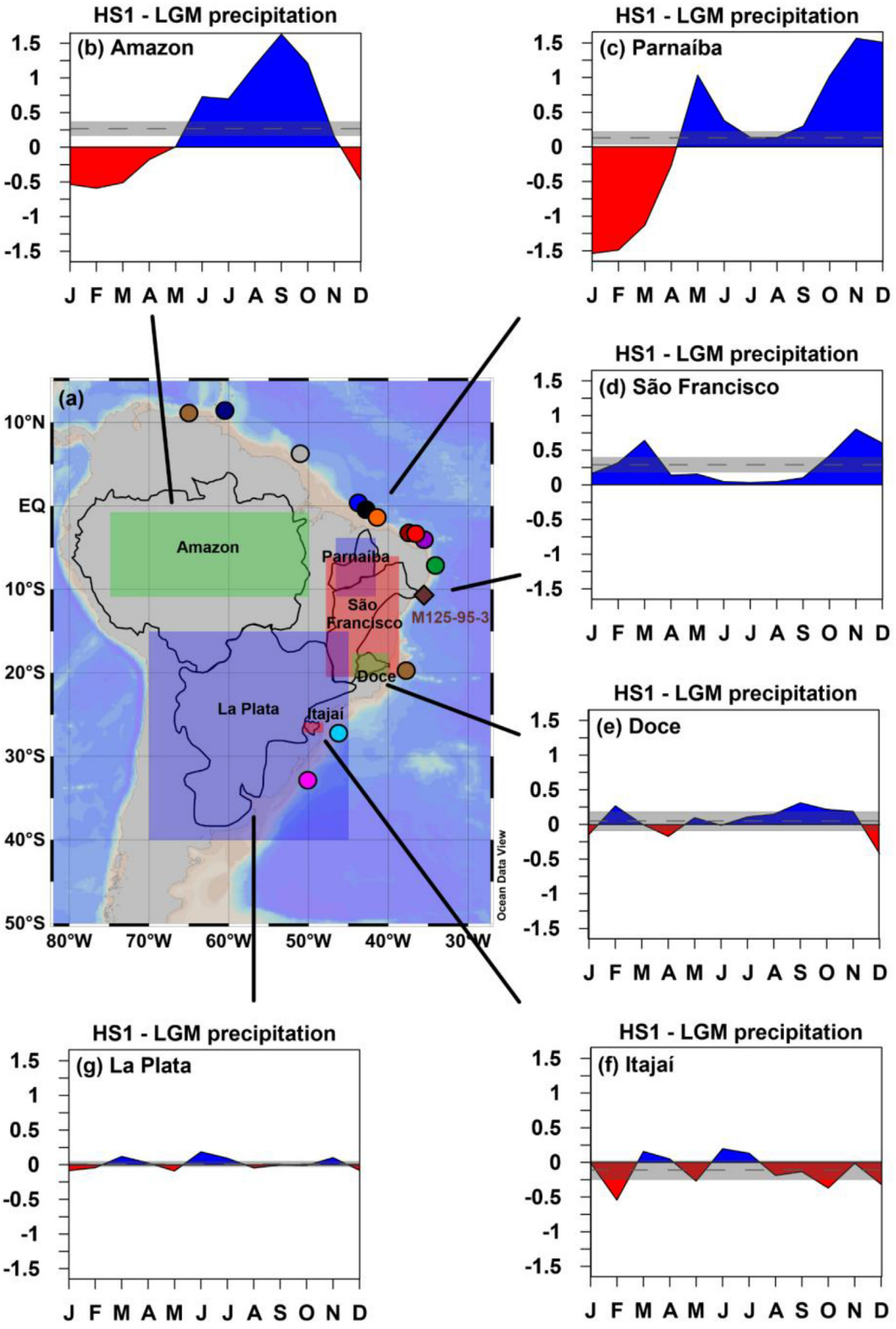

Fig. 1. **(a)** Location of piston core M125-95-3 (this study, brown diamond) and previously published marine paleoclimate records (circles) discussed herein (see Table 1 for more information). Green, blue and red rectangles show the selected regions for the computation of spatially averaged precipitation anomalies representing different (simplified) South American drainage basins (outlined and labeled in black). Panels **(b)**–**(g)** show simulated Heinrich Stadial 1 (HS1) minus Last Glacial Maximum (LGM) monthly-mean precipitation (red and blue filling) and HS1 minus LGM annual-mean precipitation (grey dashed line) with 2σ standard error (grey envelope) (mm/day) for the **(b)** Amazon River drainage basin (northwestern (NW) South America), **(c)** Parnaíba River drainage basin (northeastern (NE) South America), **(d)** São Francisco River drainage basin (eastern (E) South America), **(e)** Doce River drainage basin (southeastern (SE) South America), **(f)** Itajaí River drainage basin (SE South America), and **(g)** La Plata River drainage basin (SE South America). In the annual-mean, anomalies of rivers **(e)**–**(g)** are not significant at the 0.05 significance level. Model experiments were performed with CCSM3 (Collins et al., 2006; Prange et al., 2015). This figure was partially produced with Ocean Data View (Schlitzer, 2017). (For interpretation of the references to color in this figure legend, the reader is referred to the Web version of this article.)

Table 1
Marine sediment cores from northern (N), northwestern (NW), northeastern (NE), eastern (E) and southeastern (SE) South America investigated in this study.

Core ID	Region	Latitude	Longitude	Water depth (m)	Reference
M78/1-235-1	N South America	11.62°N	60.97°W	852	Bahr et al. (2018) and Poggemann et al. (2018)
MD03-2621	N South America	10.68°N	64.97°W	847	Deplazes et al. (2013)
GeoB16224-1	NW South America	6.66°N	52.08°W	2510	Zhang et al. (2017)
CDH86	NE South America	0.33°N	44.20°W	3107	Nace et al. (2014)
GL1248	NE South America	0.92°S	43.40°W	2264	Venancio et al. (2018)
GeoB16202-2	NE South America	1.91°S	41.59°W	2248	Mulitza et al. (2017)
GeoB3104-1	NE South America	3.67°S	37.72°W	767	Arz et al. (1998)
GeoB3912-1	NE South America	3.67°S	37.72°W	772	Arz et al. (1998)
GeoB3910-2	NE South America	4.25°S	36.35°W	2362	Jaeschke et al. (2007)
GeoB3176-1	NE South America	7.01°S	34.44°W	1385	Arz et al. (1999)
M125-95-3	E South America	10.94°S	36.20°W	1897	this study
GeoB3229-2	SE South America	19.64°S	38.72°W	780	Behling et al. (2002)
GeoB2107-3	SE South America	27.18°S	46.45°W	1048	Gu et al. (2017)
GeoB6212-1	SE South America	32.69°S	50.11°W	1010	Campos et al. (2019)

continental slope off E South America near the São Francisco River mouth during RV Meteor cruise M125 (Bahr et al., 2016) (Table 1; Fig. 1a). Since our focus relies on the abrupt millennial scale events (i.e. HS) of the last glacial (i.e. Marine Isotope Stages (MIS) 4-2), we analyzed the uppermost ca. 7.4 m of the piston core that covers the last ca. 70 ka.

We further compiled paleoclimate data from other 13 marine sediment cores collected from the Atlantic continental margin of South America spanning from 11.62°N to 32.69°S (Table 1; Fig. 1a).

3.2. Age model

The chronology of piston core M125-95-3 is based on nine planktonic foraminifera accelerator mass spectrometry (AMS) radiocarbon ages and three benthic foraminifera oxygen isotopic composition ($\delta^{18}O$) tie-points aligned to a benthic $\delta^{18}O$ reference curve from Govin et al. (2014) (Table 2; Fig. 2).

For every radiocarbon sample we hand-picked under a binocular microscope ca. 10 mg of fossil tests of planktonic foraminifera *Globigerinoides ruber* from the sediment fraction larger than 150 μm. In the absence of enough *G. ruber* tests, radiocarbon samples were completed with other planktonic foraminifera species. Samples were analyzed at the Beta Analytic Radiocarbon Dating Laboratory, USA (Table 2). Radiocarbon ages were calibrated with the IntCal13 curve (Reimer et al., 2013) with a variable simulated reservoir age from the transient modelling experiments in Butzin et al. (2017). Reservoir age and 1σ uncertainty of the simulated radiocarbon was assigned from the nearest gridbox to our core location and corresponding to our measured radiocarbon age range. Three age reversals at 100, 144, and 154 cm were not included in the age model and may be due to bioturbation bringing younger material to greater depths. Radiocarbon ages cover the uppermost 452 cm (ca. 40 ka before present (BP)) of our core.

We performed $\delta^{18}O$ analyses on 142 samples of benthic foraminifera *Uvigerina* spp. Around 10 *Uvigerina* spp. specimens per sample were handpicked under a binocular microscope from the sediment fraction larger than 125 μm. Analyses were conducted with a gas isotope ratio mass spectrometer (Finnigan MAT252) coupled to an automated carbonate preparation device (Kiel III) at the MARUM – Center for Marine Environmental Sciences, University of Bremen, Germany. Output data were calibrated against an in-house standard (Solnhofen limestone) that is itself calibrated against the NBS19 standard. Results are reported in per mil (parts per thousand, i.e. ‰) versus Vienna Pee Dee Belemnite (VPDB). Standard deviation of in-house standard replicate measurements was 0.06‰ for the measured period. The three tie-points are based on the alignment of M125-95-3 *Uvigerina* spp. $\delta^{18}O$ to a reference curve from Govin et al. (2014) (details regarding the tie-points can be found in Supplementary Material Table S1 and Fig. S1).

The age model was performed with the software PaleoDataView v. 0.8.3.4 (Langner and Mulitza, 2019) using the age modelling tool BACON v. 2.2 (Blaauw and Christen, 2011). Default parameter

Table 2
Accelerator mass spectrometer radiocarbon ages and tie-points aligned to reference curve MD95-2042 (Govin et al., 2014) used to construct the age model of piston core M125-95-3.

Depth (cm)	Lab ID	Radiocarbon age ± 1σ error (a BP)	Calibrated age (cal a BP)	Tie-point age ± estimated error (a BP)
6	462829	1940 ± 30	1472	
54	479391	8390 ± 30	8892	
84	490135	12270 ± 30	13638	
100	462830	8310 ± 40	[a]	
144	490136	10700 ± 30	[a]	
154	479392	7360 ± 30	[a]	
200	462831	17820 ± 60	20701	
254	479393	21440 ± 60	24816	
308	490137	25160 ± 90	28443	
340	462832	27620 ± 150	30898	
400	462833	32170 ± 220	35372	
452	479395	35180 ± 230	39087	
498				47000 ± 2141
582				59300 ± 2049
738				71100 ± 2137

[a] Radiocarbon age reversals that were not included in the age model.

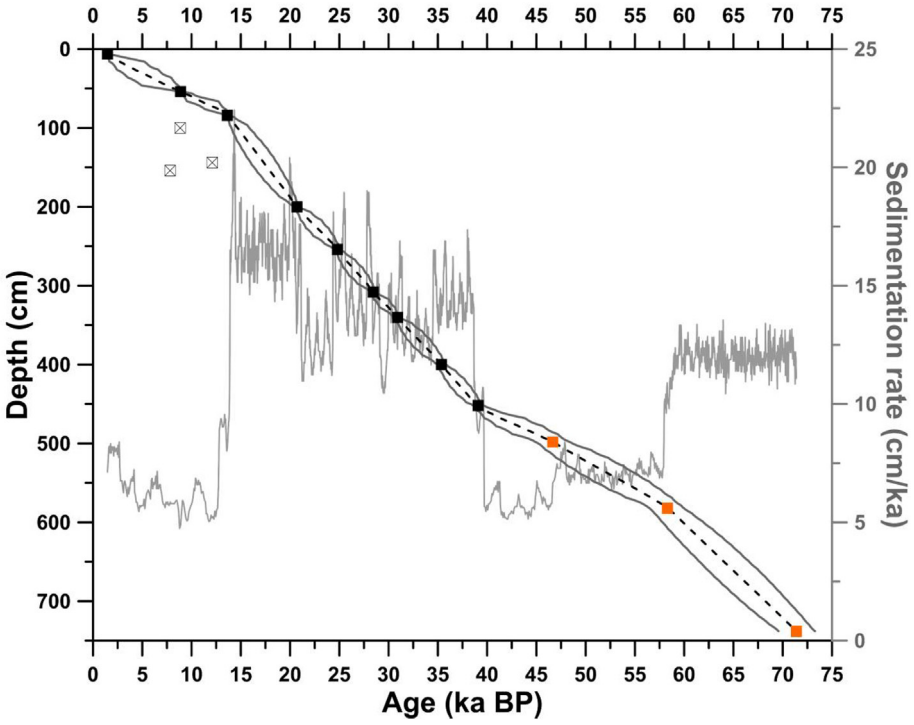

Fig. 2. Age model (black dashed line and enveloping curves) and sedimentation rates (grey line) for piston core M125-95-3 produced with software PaleoDataView v. 0.8.3.4 (Langner and Mulitza, 2019) using the age modelling tool BACON v. 2.2 (Blaauw and Christen, 2011). For the age model, the black (orange) squares depict calibrated radiocarbon ages (tie-points), the dashed line depicts median ages, and the upper (lower) black line depicts maximum (minimum) ages. Open crossed squares are age reversals. (For interpretation of the references to color in this figure legend, the reader is referred to the Web version of this article.)

settings were used, except for mem.mean (set to 0.4) and mean.-strength (set to 4). 10,000 realizations and a *t*-distribution with 9 degrees of freedom (t.a = 9, t.b = 10) were applied. All ages are reported as years (a) BP (present is 1950 AD).

3.3. Major element composition

X-ray fluorescence (XRF) core scanner data were collected every 5 mm down-core over a 0.6 cm^2 area with down-core slit size of 5 mm using generator settings of 10 kV, a current of 0.065 mA and a sampling time of 8 s. Analyses were performed at the surface of u-channels sampled from the archive half of piston core M125-95-3. We used the XRF Core Scanner III (AVAATECH Serial No. 12) at the MARUM – Center for Marine Environmental Sciences, University of Bremen, Germany. The surface of the u-channels was covered with a 4 μm thin SPEXCerti Prep Ultralene1 foil to avoid contamination of the XRF measurement unit and desiccation of the sediment. The herein reported data have been acquired by a SGX Sensortech Silicon Drift Detector (Model SiriusSD® D65133Be-INF with 133eV X-ray resolution), a Topaz-X High- Resolution Digital MCA and an Oxford Instruments 100W Neptune X-Ray tube with rhodium (Rh) target material. Raw data were processed by the analysis of X-ray spectra by iterative least square software (WIN AXIL) package from Canberra Eurisys.

Dried and homogenized powder samples analyzed via energy dispersive polarized XRF (EDP-XRF) has been proven useful to verify XRF core scanner elemental intensities in an efficient way (Tjallingii et al., 2007). Thus, we also analyzed elemental concentrations by EDP-XRF on bulk sediment samples from the working half every 20 cm. Around 10 cm^3 of sample were freeze-dried and homogenized with a hand agate mortar. We replicated 10% of the samples in order to check the efficiency of the sample preparation and the equipment reproducibility (sd: 2.7% Ca; 2.6% Ti; 3.2% Fe; 1.8% K). Analyses were performed at the Fluminense Federal University, Brazil.

In order to capture changes in the input of terrigenous inorganic sediments to our core site (and, thus, precipitation over São Francisco River drainage basin) as well as changes in chemical weathering over the São Francisco River drainage basin we use ln(Ti/Ca) and ln(Fe/K), respectively (Govin et al., 2012; Mulitza et al., 2008). The less commonly used ln(Fe/K) ratio is based on the different mobility of both elements during chemical weathering. Since potassium is much more mobile than iron, high ln(Fe/K) values indicate intense chemical weathering.

3.4. Climate model experiment

We analyzed the results from a freshwater hosing experiment (0.2 Sv injected into the northern North Atlantic for 400 years resulting in a ~50% weakening of the AMOC from about 12 Sv to 6 Sv) conducted under full Last Glacial Maximum (LGM) background climatic conditions (following the protocol of the Paleoclimate Modelling Intercomparison Project Phase 2, for details see Erokhina et al. (2017)) mimicking HS1 (Prange et al., 2015). The atmosphere-ocean general circulation model CCSM3 (Collins et al., 2006) in the high-resolution version T85 (1.4° atmosphere transform grid; ocean grid resolution nominal 1°) was used. Therefore, the model resolution used in this study is much higher than in previous LGM hosing studies; e.g. in the multi-model study by Kageyama et al. (2013) atmospheric grid resolutions ranged from T21 (5.6° transform grid) to T42 (2.8° transform grid). Analysis is based on annual-mean and seasonal-mean (extended austral summer, November–March; extended austral winter, May–September) climatologies calculated from 50-year averages. Additionally, we calculated

the monthly-mean precipitation differences (HS1 minus LGM) for the Amazon, Parnaíba, São Francisco, Doce, Itajaí and La Plata River drainage basins (simplified catchment areas depicted in Fig. 1a).

4. Results

4.1. Age model

The uppermost 7.4 m of core M125-95-3 covers the last ca. 70 ka, i.e. since MIS4, with a mean sedimentation rate of 11.9 cm/ka (Fig. 2). The lowest sedimentation rate (4.7 cm/ka) occurs within the early MIS1 (ca. 8.8 ka BP) while the highest value (22.4 cm/ka) was recorded within MIS2 (ca. 14.4 ka BP) (Fig. 2).

4.2. Oxygen isotopic composition of benthic foraminifera

Uvigerina spp. $\delta^{18}O$ ranges from 2.63 to 5.02‰ (Fig. 3c). The lowest value occurs during the late Holocene around 3.4 ka BP (MIS1) while the highest value occurs during the LGM around 19.3 ka BP (MIS2). The final stage of the glacial inception, i.e. the transition from MIS5a to MIS4, is located at the base of our record around 70 ka BP. MIS4 is marked by a gradual decrease in $\delta^{18}O$ values that peaks around 59 ka BP. During MIS3, relative low values around 47 ka BP are coeval with HS5. MIS2 shows a gradual trend towards higher $\delta^{18}O$ values. The last deglaciation is marked by two major sharp decreases in $\delta^{18}O$ around 18.4 and 11.5 ka BP, synchronous (within age model uncertainties) to HS1 and the Younger Dryas (YD).

4.3. Major element composition

XRF core scanner ln(Ti/Ca) values (expressed as count ratios) vary between −3.88 and 1.46 (Fig. 3b). Positive peaks during MIS4-2 are coeval with HS of the last glacial (i.e. HS6-YD), while the lowest values occur during the early Holocene. XRF core scanner ln(Fe/K) values range from 1.23 to 2.47 and the highest values occur during MIS1 (around the YD) (Fig. 3a). ln(Fe/K) values also increase during HS, but increases show lower relative magnitude compared to increases in ln(Ti/Ca). EDP-XRF ln(Ti/Ca) values vary between −3.83 and 0.51 (Fig. 3b) and EDP-XRF ln(Fe/K) between 1 and 1.36 (Fig. 3a). XRF core scanner and EDP-XRF values show similar trends.

4.4. Climate model experiment

Annual-mean HS1 minus LGM precipitation (Fig. 4a) shows positive anomalies over most of tropical South America except for N South America, which exhibits negative anomalies. SE South America shows no major change in precipitation. Seasonal-mean HS1 minus LGM precipitation (Fig. 4b and c) shows a southward shifted ITCZ and a meridional rainfall anomaly dipole over tropical South America, during both austral summer and winter. The dipole pattern is restricted to E South America between ca. 0° and 20°S during austral summer, and shifts further north, about the equator between ca. 10°N and 10°S, during austral winter. SE South America, in turn, shows no major change in precipitation in either season except for an austral summer negative anomaly over its western portion.

Seasonal-mean HS1 minus LGM surface temperature (Fig. 5a and b) shows, in general, negative (positive) anomalies in the

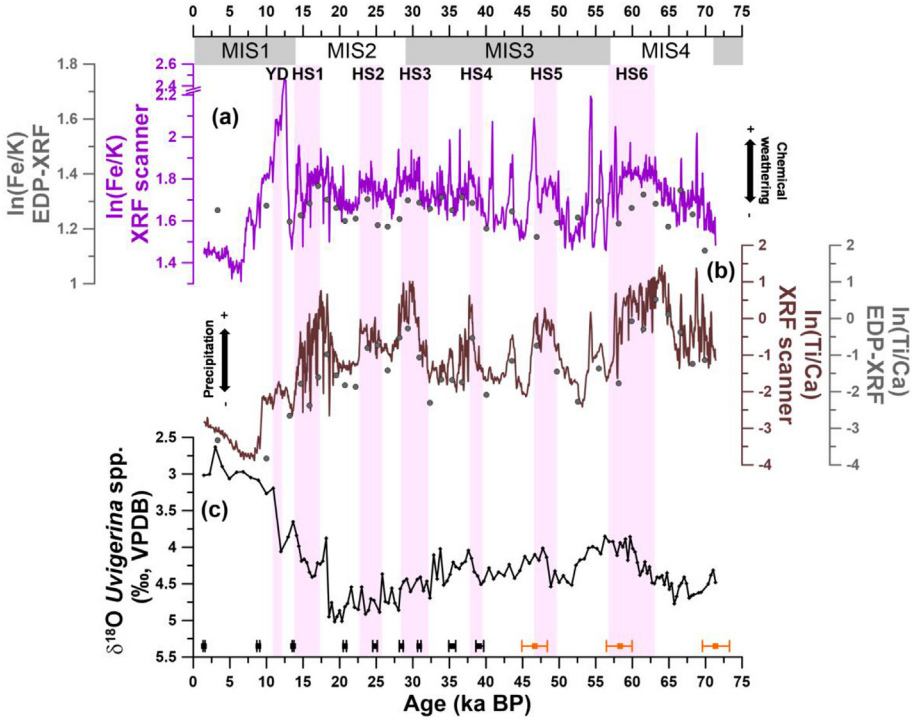

Fig. 3. Isotopic and geochemical records from piston core M125-95-3 for the last ca. 70 ka. **(a)** X-ray fluorescence (XRF) core scanner ln(Fe/K) (purple line; the axis was broken from 2.2 to 2.4) and energy dispersed polarized (EDP) XRF ln(Fe/K) (grey circles); **(b)** XRF core scanner ln(Ti/Ca) (brown line) and EDP-XRF ln(Ti/Ca) (grey circles); and **(c)** *Uvigerina* spp. stable oxygen isotopic composition ($\delta^{18}O$). Black (orange) squares at the bottom of the panel depict calibrated radiocarbon ages (tie-points) with 2σ standard error. Pink vertical bars represent abrupt millennial scale events Younger Dryas (YD) and Heinrich Stadial (HS) 1 to 6. Marine Isotope Stages (MIS) are depicted below the upper axis. (For interpretation of the references to color in this figure legend, the reader is referred to the Web version of this article.)

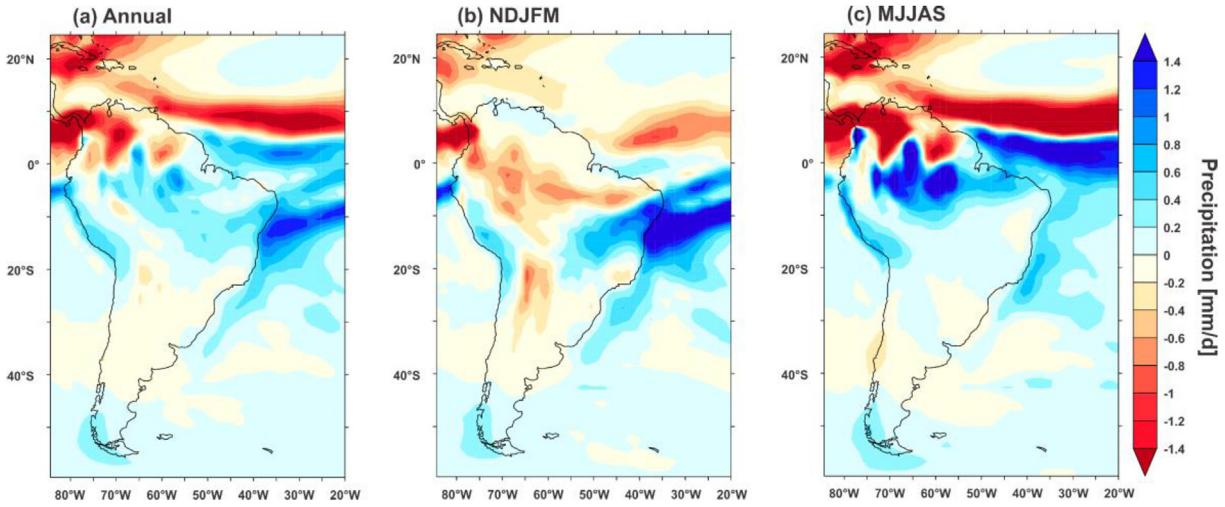

Fig. 4. Heinrich Stadial (HS) 1 minus Last Glacial Maximum (LGM) precipitation simulated with CCSM3. **(a)** Annual-mean, **(b)** extended austral summer (i.e. November–March (NDJFM)), and **(c)** extended austral winter (i.e. May–September (MJJAS)) rainfall.

Northern Hemisphere (Southern Hemisphere) during both seasons. Seasonal-mean HS1 minus LGM total precipitable water (Fig. 5c and d) shows strong negative (positive) anomalies over the North Atlantic (South Atlantic) also during both seasons, thermodynamically linked to temperature anomalies. In addition, during austral summer (Fig. 5c), there are negative (positive) anomalies in precipitable water over N, NW and SE (NE and E) South America. During austral winter (Fig. 5d), on the other hand, a widespread positive anomaly in precipitable water dominates tropical South America to the south of the equator. The HS1 minus LGM low level circulation (i.e. 900 hPa) (Fig. 5a and b) shows wind anomalies with a northerly component over tropical South America during both seasons. Austral summer HS1 minus LGM moisture transport (Fig. 5c) shows an anomalous cyclonic pattern over E South America resulting in enhanced ocean-continent moisture transport south of ca. 15°S. During austral winter (Fig. 5d), more moisture from the equatorial Atlantic enters tropical South America. Absolute moisture transport for the LGM is shown in the supplementary material (Fig. S2).

Monthly-mean HS1 minus LGM precipitation over the drainage basins depicted in Fig. 1a indicates that the Amazon (i.e. 0.27±0.10 mm/day), Parnaíba (i.e. 0.13±0.10 mm/day) and São Francisco (i.e. 0.29±0.11 mm/day) River drainage basins experience marked positive precipitation anomalies, while the Doce (i.e. 0.05±0.14 mm/day), Itajaí (i.e. −0.11±0.14 mm/day) and La Plata (i.e. 0.01±0.04 mm/day) River drainage basins show no significant differences (Fig. 1b–g). We note that the magnitude of the modeled precipitation anomalies may depend on the strength of the AMOC perturbation.

5. Discussion

5.1. The marine paleoclimate record of changes in precipitation over (sub-) tropical South America during HS

Marine paleoclimate archives consistently recorded tropical precipitation changes during last glacial HS over N (Bahr et al., 2018; Deplazes et al., 2013), NW (Zhang et al., 2017) and NE (Arz et al., 1999, 1998; Jaeschke et al., 2007; Mulitza et al., 2017; Nace et al., 2014; Venancio et al., 2018) South America (Fig. 6a–j). These archives recorded the response of fluvial discharge to changes in precipitation over specific drainage basins. During HS, they suggest dry conditions over N South America (Bahr et al., 2018; Deplazes et al., 2013) and wet conditions over NW (Zhang et al., 2017) and NE (Arz et al., 1999, 1998; Jaeschke et al., 2007; Mulitza et al., 2017; Nace et al., 2014; Venancio et al., 2018) South America. This pattern agrees with a previously suggested southward migration of the ITCZ and tropical rain belt (e.g. Broccoli et al., 2006; Schneider et al., 2014) that is corroborated by our simulated HS1 minus LGM annual-mean precipitation pattern (Fig. 4a). Additionally, our monthly-mean HS1 minus LGM precipitation results (Fig. 1b and c) further support the positive precipitation anomalies suggested for the Amazon and Parnaíba River drainage basin cores (Fig. 6c–f).

On the other hand, marine paleoclimate archives collected to the south of 20°S off SE South America (Behling et al., 2002; Campos et al., 2019; Gu et al., 2017) (Fig. 6l–n) show no changes in terrigenous input during last glacial HS, suggesting that precipitation anomalies over those drainage basins were not intense enough to produce increased fluvial discharge to the SE South American continental margin. Indeed, our annual and monthly mean HS1 minus LGM precipitation results show no major anomalies over the drainage basins of the Doce, Itajaí and La Plata Rivers (Fig. 1e–g; 4a).

Our marine paleoclimate archive (i.e. 10.94°S, off E South America, Fig. 6k) fills the gap between the presence of HS signals recorded in marine records to the north of 7°S and the absence of HS signals recorded by marine records to the south of 20°S. It shows recurrent peaks in ln(Ti/Ca) during the last glacial period suggesting systematic increases in the discharge of terrigenous sediments by the São Francisco River to the adjacent continental margin during HS6-YD. In addition, our model results show positive precipitation anomalies over the São Francisco River drainage basin (Fig. 1d; 4a). We suggest that E South America experienced positive precipitation anomalies during all HS of the last glacial. Our new archive is the first marine record off E South America and the southernmost from the Atlantic continental margin of South America to consistently record increased precipitation over E South America during HS. Additionally, our ln(Fe/K) data varies coevally with our ln(Ti/Ca) record, supporting our suggestion that the increases in ln(Ti/Ca) were indeed associated to increased continental precipitation (Fig. 3a). Higher ln(Fe/K) values indicate enhanced

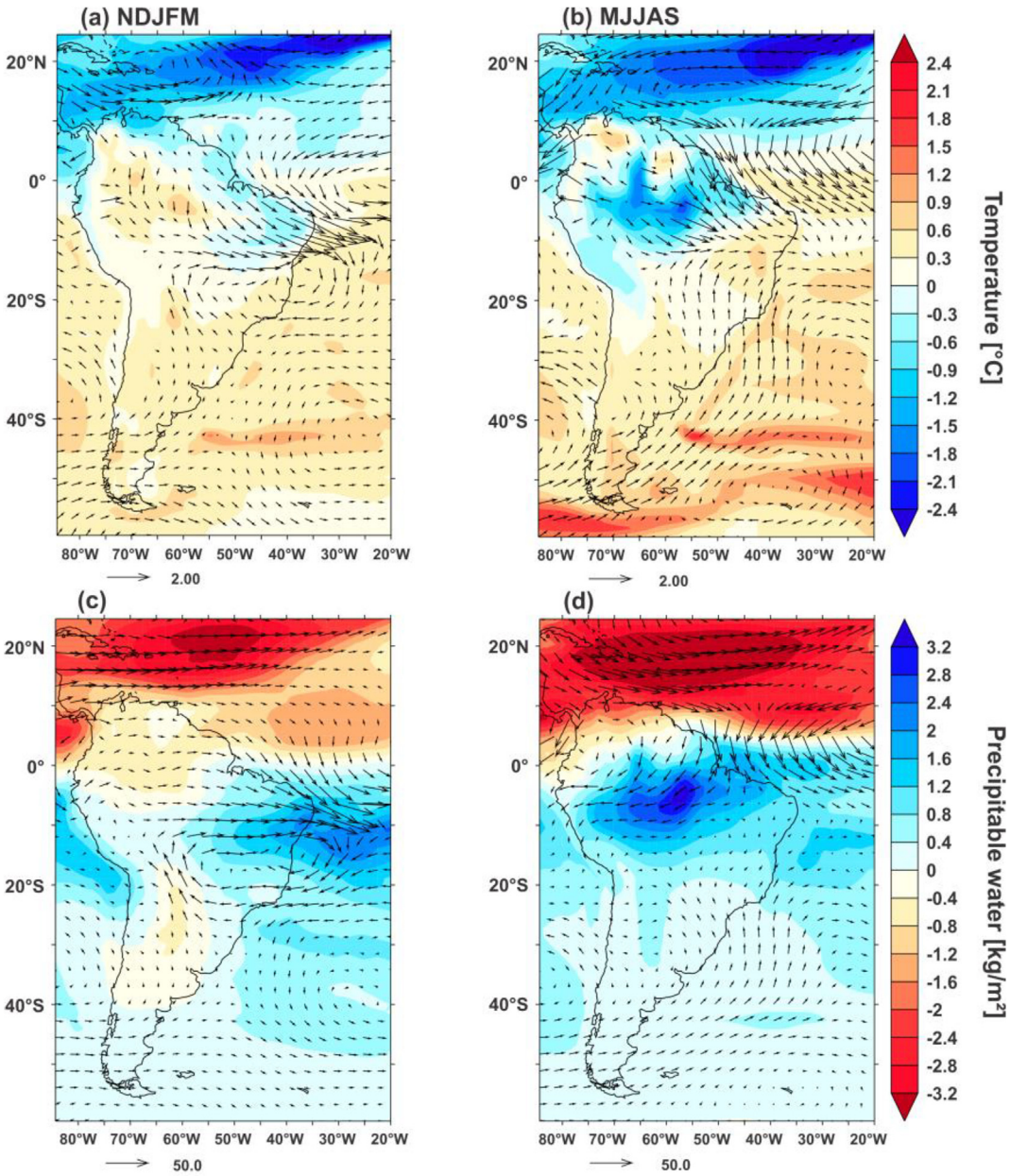

Fig. 5. Heinrich Stadial (HS) 1 minus Last Glacial Maximum (LGM) seasonal-mean surface temperature and total precipitable water along with 900 hPa winds (m/s) and vertically integrated moisture transport (kg/(m·s)) simulated with CCSM3. **(a)** Extended austral summer (i.e. November–March (NDJFM)) surface temperature and 900 hPa wind; **(b)** extended austral winter (i.e. May–September (MJJAS)) surface temperature and 900 hPa wind; **(c)** extended austral summer (i.e. NDJFM) precipitable water and moisture transport; and **(d)** extended austral winter (i.e. MJJAS) precipitable water and moisture transport. Only every 2nd vector in each direction is plotted.

chemical weathering (Govin et al., 2012; Mulitza et al., 2008), likely caused by increased precipitation over the São Francisco River drainage basin.

The meridional impact of HS-induced precipitation anomalies over South America seems to decrease from north to south (Fig. 6). The N (Fig. 6a and b), NW (Fig. 6c) and NE (Fig. 6d–j) South American cores recorded HS with signals of large amplitude. Our record (i.e. E South American; Fig. 6k) still shows marked HS-signals but of lower amplitude. Conversely, the SE South American cores (Fig. 6l–n) have not responded to HS. A decreasing amplitude in HS-related signal is also evident in our model results (Fig. 1b–g; 4a). Our record also shows a long-term trend that seems to be driven by the combination of sea level and orbital changes. A similar long-term trend can also be identified in SE South American cores (Fig. 6l–n). Indeed, Gu et al. (2017) related the long-term trend present in their ln(Fe/Ca) record (Fig. 6m) to changes in sea level and orbital obliquity. The high magnitude of the HS signal captured by the N, NW and NE South American archives may have dampened the long-term trend. Since our focus here relies on the abrupt millennial scale events of the last glacial, a detailed discussion regarding orbital scale signals is out of our scope.

5.2. The continental paleoclimate record of changes in precipitation over (sub-) tropical South America during HS

Tropical South American archives consistently recorded last

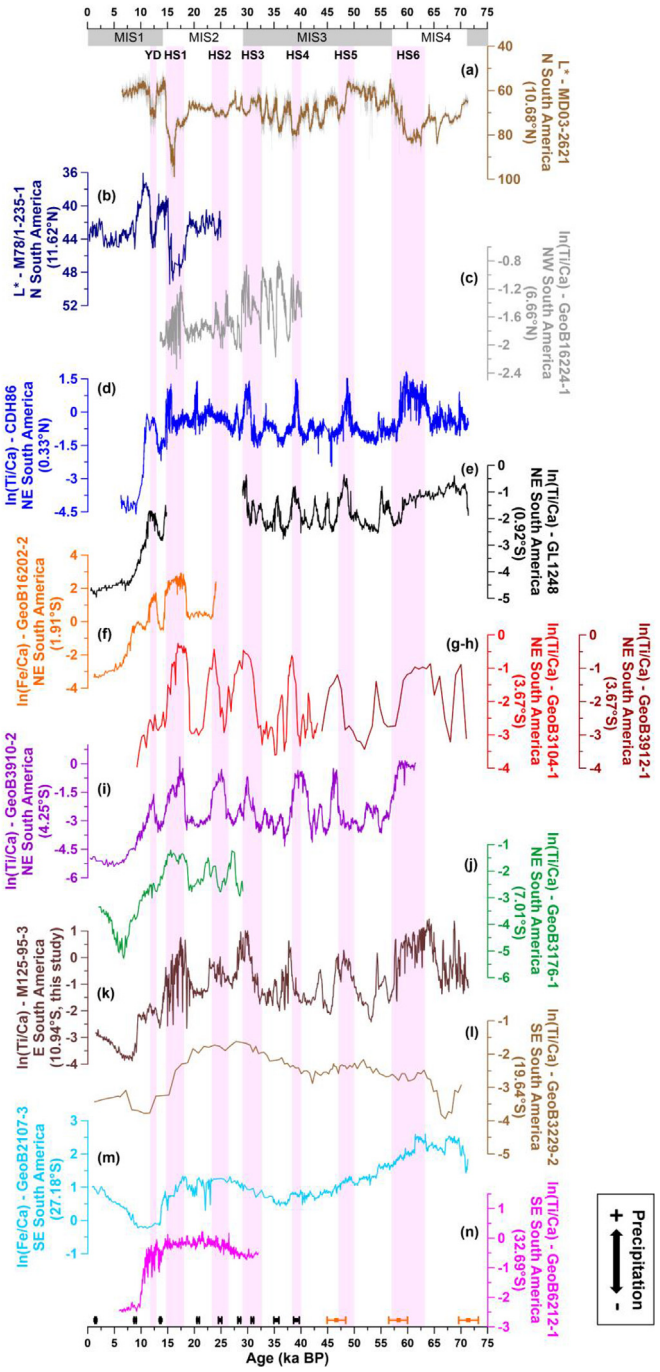

Fig. 6. Marine paleoclimate records from the Atlantic continental margin of South America (color coded according to Fig. 1a). **(a)** Lightness (L*) from northern (N) South American core MD03-2621 (Deplazes et al., 2013) (brown line represents a 399-point running average); **(b)** L* from N South American core M78/1-235-1 (Bahr et al., 2018; Poggemann et al., 2018); **(c)** ln(Ti/Ca) from core GeoB16224-1 that represents northwestern (NW) South American (Zhang et al., 2017); **(d)** ln(Ti/Ca) from northeastern (NE) South American core CDH86 (Nace et al., 2014); **(e)** ln(Ti/Ca) from NE South American core GL1248 (Venancio et al., 2018); **(f)** ln(Fe/Ca) from NE South American core GeoB16202-2 (Mulitza et al., 2017); **(g)** ln(Ti/Ca) from NE South American core GeoB3104-1 (Arz et al., 1998); **(h)** ln(Ti/Ca) from NE South American core GeoB3912-1 (Arz et al., 1998); **(i)** ln(Ti/Ca) from NE South American core GeoB3910-2 (Jaeschke et al., 2007); **(j)** ln(Ti/Ca) from NE South American core GeoB3176-1 (Arz et al., 1999); **(k)** ln(Ti/Ca) from eastern (E) South American core M125-95-3 (this study); **(l)** ln(Ti/Ca) from southeastern (SE) South American core GeoB3229-2 (Behling et al., 2002); **(m)** ln(Fe/Ca) from SE South American core GeoB2107-3 (Gu et al., 2017); and **(n)** ln(Ti/Ca) from SE South American core GeoB6212-1 (Campos et al., 2019). Black (orange) squares at the bottom of the panel depict calibrated radiocarbon ages (tie-points) with 2σ standard error. Pink vertical bars represent abrupt millennial scale climate change events Younger Dryas (YD) and Heinrich Stadial (HS) 1 to 6. Marine Isotope Stages (MIS) are depicted below the upper axis. (For interpretation of the references to color in this figure legend, the reader is referred to the Web version of this article.)

glacial HS induced precipitation anomalies related to the southward migration of the ITCZ (e.g. Baker et al., 2001; Kanner et al., 2012; Zular et al., 2019). These anomalies are negative over N South America (Zular et al., 2019) and positive over NW (Baker et al., 2001; Kanner et al., 2012) and NE (Cruz et al., 2009; Ledru et al., 2006) South America. The anomalies recorded by N, NW and NE hydroclimate reconstructions are largely supported by previous modelling studies (e.g. Broccoli et al., 2006; Kageyama et al., 2013) as well as by our model results for annual-mean HS1 minus LGM precipitation (Fig. 4a). Also, our monthly-mean HS1 minus LGM precipitation results (Fig. 1b and c) further corroborate the positive precipitation anomalies recorded by NW and NE South American records (e.g. Baker et al., 2001; Cruz et al., 2009; Kanner et al., 2012). Hydroclimate records from E South America (e.g. Stríkis et al., 2018; Wang et al., 2004) also show positive precipitation anomalies during HS of the last glacial and are equally supported by previous modelling studies (e.g. Broccoli et al., 2006; Kageyama et al., 2013) as well as by our modeled HS1 minus LGM precipitation (Fig. 1c; 4a).

The scenario over SE South America is not as clear as the one over N, NW, NE and E South America. SE South American records with appropriate resolution to capture HS of the last glacial mainly stem from stalagmites (Cruz et al., 2005; Hessler et al., 2010; Wang et al., 2006). Stalagmite $\delta^{18}O$ (and local precipitation $\delta^{18}O$) are mainly affected by moisture source, amount of rainfall and temperature. Based on modern conditions, millennial scale negative anomalies in the $\delta^{18}O$ of stalagmites from SE South America (e.g. Botuverá cave (27.22°S) and Santana cave (24.53°S)) were first related to an increase in the intensity of the SAMS, which is one of the moisture sources to SE South America (i.e. source effect) (Cruz et al., 2005).

Later, trace elements (i.e. Mg/Ca and Sr/Ca) from a Botuverá cave stalagmite were used as a proxy for the local amount of rainfall (Cruz et al., 2007). Since the authors identified a positive correlation between stalagmite trace element ratios and $\delta^{18}O$ for the whole record on orbital scale, they reassessed previous (Cruz et al., 2005) interpretations suggesting that periods of negative $\delta^{18}O$ anomalies (lower trace element ratios) in the stalagmites were not only related to moisture source (^{18}O-depleted moisture transported from the Amazon basin towards SE South America), but also to higher amount of local precipitation in response to a stronger SAMS (i.e. a mixture of source and local amount effects). However, despite the stalagmite $\delta^{18}O$ negative anomalies, the positive correlation with trace elements is not clear on millennial scale, hindering a conclusive statement about the mechanism (source effect, local amount effect, or both) controlling the $\delta^{18}O$ negative anomalies on SE South American stalagmites during HS. Recently, Millo et al. (2017) analyzed the isotopic composition of fossil dripwater from a Botuverá cave stalagmite and suggested that the $\delta^{18}O$ of SE South American stalagmites is not appropriate for quantitative (local amount effect) interpretations.

By using a water isotope-enabled general circulation model, Lewis et al. (2010) simulated precipitation $\delta^{18}O$ for HS-like conditions and classified the caves from SE South America as dominated by local amount effect. However, the authors indicated that the transport of ^{18}O-depleted moisture from the Amazon basin towards SE South America during periods of strong SAMS also contributed to the low $\delta^{18}O$ of local precipitation (moisture source effect).

Non-speleothem paleoclimate archives from SE South America

(Behling et al., 2002; Campos et al., 2019; Gu et al., 2017) do not record the hydroclimate signal of HS of the last glacial, indicating that if local precipitation increased during HS, these anomalies were not intense enough to produce increased fluvial discharge to the continental margin (Fig. 6l–n). The records from Behling et al. (2002), Campos et al. (2019) and Gu et al. (2017) are supported by previous numerical simulations (Kageyama et al., 2013; Mohtadi et al., 2016). Also, our annual and monthly mean HS1 minus LGM precipitation results (Fig. 1e–g; 4a) show a reduction in the intensity of precipitation anomalies from tropical to subtropical South America, reinforcing our suggestion of a north-south decrease in the meridional impact of HS-induced precipitation anomalies over South America.

Importantly, El Niño–Southern Oscillation (ENSO) is known to influence variability of the La Plata River discharge (Piola et al., 2005). However, since (i) marine sediment cores from the continental slope usually have no appropriate temporal resolution to address interannual variability (e.g. Zhang et al., 2015) and (ii) reconstructions of ENSO variability are not well established during HS for both paleorecords (Felis et al., 2012; Koutavas et al., 2002; Leduc et al., 2009) and numerical simulations (Liu et al., 2014; Merkel et al., 2010), we refrain addressing any ENSO impacts on South American precipitation during HS.

5.3. A new mechanism for precipitation changes over tropical South America

The annual-mean HS1 minus LGM precipitation anomaly (Fig. 4a) apparently corroborates the mechanism usually invoked to explain the increase in precipitation over tropical South America to the south of the equator during HS of the last glacial (Kanner et al., 2012; Peterson et al., 2000; Stríkis et al., 2015). According to this mechanism, an austral summer enhanced SAMS was accompanied by the southward migration of the ITCZ and a strong SACZ (Cruz et al., 2005; Kanner et al., 2012; Peterson et al., 2000; Stríkis et al., 2015). However, the detailed analyses of the seasonal-mean HS1 minus LGM anomalies from our model experiment (Fig. 4b and c; 5) suggests a different mechanism. The annual-mean pattern results from a complex combination of the individual seasonal response patterns, which involves dynamic and thermodynamic processes.

In modern climate, a strong AMOC promotes an oceanic northward net cross-equatorial energy transport. To compensate this inter-hemispheric asymmetry, the net cross-equatorial energy transport performed by the atmosphere is directed southward (Marshall et al., 2014; Mohtadi et al., 2016). To accomplish that, the location of the ascendant branch of the Hadley cell and, thus, the ITCZ are placed to the north of the equator. However, during HS of the last glacial, a substantially weaker or disrupted AMOC would decrease the northward ocean heat transport and induce a weakening or reversal of the atmospheric cross-equatorial energy transport. In response, a cooling (warming) of the North Atlantic (South Atlantic) and a reorganization of the global Hadley cell would occur, promoting a southward ITCZ shift (Broccoli et al., 2006; Mohtadi et al., 2016; Mulitza et al., 2017; Schneider et al., 2014). In association with the migration of the ITCZ, a meridional rainfall anomaly dipole emerges over tropical South America (Fig. 4) and can be considered the continental counterpart of the marine ITCZ shift. During austral summer (winter), the dipole is located between ca. 0° and 20°S (10°N and 10°S) (Fig. 4b and c). This precipitation dipole is primarily a dynamic response to cooling (warming) of the Northern Hemisphere (Southern Hemisphere) and associated with northerly low-level wind anomalies that are generally directed along surface temperature gradients (Fig. 5a and b) (cf. Lindzen and Nigam, 1987).

In addition to this dynamic response, thermodynamic processes also play an important role in setting up tropical South American precipitation during HS of the last glacial. During austral summer (winter), the North Atlantic (South Atlantic) is the main source of moisture for tropical South America via prevailing NE trade winds (SE trade winds) (Fig. S2). Due to the HS cooling of the North Atlantic the atmospheric moisture content over the Northern Hemisphere is reduced (Fig. 5c and d). Consequently, in austral summer cooler and drier air is transported by the prevailing NE trade winds (Fig. S2; 5c) from the tropical North Atlantic into the continent, resulting in reduced transport of moisture to feed rainfall over tropical South America. Moreover, cooler and drier low-level NE trade winds transport less moist static energy into the continent. A resulting decrease in low-level moist static energy stabilizes the atmospheric vertical column and inhibits convection (Cook and Vizy, 2006; Neelin and Held, 1987).

Thus, differently from previous suggestions (e.g. Kanner et al., 2012; Peterson et al., 2000; Stríkis et al., 2015), last glacial HS austral summers were characterized by drier conditions over vast tropical South American regions, including the Amazon and the northern portion of the Parnaíba River drainage basins (Figs. 1b, c and 4b). Increased austral summer rainfall over E South America between ca. 15°S and 25°S is associated with an anomalous cyclonic circulation and moisture transport from the anomalously warm South Atlantic into the continent (Fig. 4b; 5c).

Last glacial HS austral winters show wetter conditions prevailing over most tropical South America to the south of the equator (Fig. 4c). During austral winters, enhanced precipitation over the western Amazon (ca. 0°-10°S) is fed by moisture from the eastern Amazon region and the equatorial North Atlantic (Fig. 5d). Positive SST anomalies in the eastern equatorial Pacific, likely a response to the weakened AMOC during HS, have been reported to enhance western Amazon precipitation by promoting a regional easterly low-level wind anomaly and moisture recycling from the central Amazon towards the Andes (Timmermann et al., 2007; Zhang et al., 2016). The São Francisco, Doce, Itajaí and La Plata River drainage basins are not affected by these anomalous moisture transports (Fig. 1d–g; 4c). It is worth noting that our model simulates enhanced precipitation over the central Andes (Fig. 4) in line with multiple HS proxy records (e.g. Zhang et al., 2016).

Therefore, our new mechanism explains that the positive precipitation anomalies that occurred over the São Francisco River drainage basin during HS of the last glacial were related to an austral summer tropical South Atlantic moisture flux instead of an austral summer intensified SACZ. Also, our model experiments give no support to a mechanism that invokes an austral summer enhanced SAMS as responsible for wetter conditions over the Amazon basin and further south during HS. Instead, we propose an austral winter equatorial Atlantic moisture flux as a source of additional rainfall (Fig. 5d). Furthermore, this new mechanism contradicts the suggested relationship between stronger SAMS convective activity over the Amazon basin, transference of the low $\delta^{18}O$ signal towards SE South America and increased local amount of rain.

6. Conclusions

Our core collected at 10.94°S contributes to reduce the gap of marine paleoclimate records between 7°S and 20°S off E South America. It is the first marine archive off E South America and the southernmost from the Atlantic continental margin of South America that consistently records the hydroclimate signal of HS of the last glacial. Our core suggests positive precipitation anomalies

over the São Francisco River drainage basin during HS6-YD. Based on new data from our core, a thorough compilation of previously available marine paleoclimate records and results from a high-resolution atmosphere-ocean general circulation model, we show that the HS-induced positive precipitation anomalies over (sub-) tropical South America to the south of the equator is latitude-dependent, decreasing from north to south. Also, we propose a new mechanism responsible for the HS positive precipitation anomalies over tropical South America to the south of the equator. During HS austral summers, cooler and drier air was transported from the tropical North Atlantic into tropical South America via prevailing NE trade winds. Consequently, drier conditions prevailed over tropical South America. An exception is made for E South America, that was affected by anomalous tropical South Atlantic cyclonic circulation. During HS austral winters, enhanced moisture was transported from the equatorial Atlantic into tropical South America. Wetter conditions occurred over most of tropical South America to the south of equator. The new mechanism proposed herein highlights the need of a broad approach to explain South American HS hydroclimate conditions that goes beyond changes in SAMS. Dynamic and thermodynamic processes, seasonal changes as well as the tropical Atlantic moisture source played crucial roles in setting up millennial scale precipitation anomalies over tropical South America.

Acknowledgements

We thank two anonymous reviewers for their comments and suggestions that improved the manuscript. Logistic and technical assistance was provided by the captain and crew of the R/V Meteor. New data shown herein are archived in Pangaea (doi:10.1594/PANGAEA.905181). M.C. Campos acknowledges the financial support from FAPESP (grants 2016/10242-0 and 2018/06790-7). C.M. Chiessi and A.L. Albuquerque acknowledges the financial support from FAPESP (grant 2018/15123-4), CAPES (grants 564/2015 and 88881.313535/2019-01), CNPq (grants 302607/2016-1, 422255/2016-5, 302521/2017-8 and 429767/2018-8) and the Alexander von Humboldt Foundation. CAPES (grants 88887.156152/2017-00 and 88881.161151/2017-01) and CNPq (grant 406322/2018-0) currently support I.M. Venancio. S. Mulitza, M. Prange, H. Kuhnert and A. Paul were funded through the DFG Research Center, Cluster of Excellence “The Ocean in the Earth System”. Support from the German PalMod initiative (BMBF) is also acknowledged. The CCSM3 simulations were performed on the supercomputer of the Norddeutscher Verbund für Hoch-und Höchstleistungsrechnen (HLRN). Sample material was provided by the Core Repository at the Fluminense Federal University, Brazil. This research used data acquired at the XRF Core Scanner Lab at the MARUM – Center for Marine Environmental Sciences, University of Bremen, Germany.

Appendix A. Supplementary data

Supplementary data to this article can be found online at https://doi.org/10.1016/j.quascirev.2019.105990.

References

Arz, H.W., Pätzold, J., Wefer, G., 1999. Climatic changes during the last deglaciation recorded in sediment cores from the northeastern Brazilian Continental Margin. Geo Mar. Lett. 19, 209–218. https://doi.org/10.1007/s003670050111.

Arz, H.W., Pätzold, J., Wefer, G., 1998. Correlated millennial-scale changes in surface hydrography and terrigenous sediment yield inferred from last-glacial marine deposits off northeastern Brazil. Quat. Res. 50, 157–166. https://doi.org/10.1006/qres.1998.1992.

Bahr, A., Albuquerque, A.L.S., Ardenghi, N., Batenburg, S.J., Bayer, M., Catunda, M.C., Conforti, A., Dias, B., Ramos, R.D., Egger, L.M., Evers, F., Fischer, T., Hatsukano, K., Hennrich, B., Hoffmann, J., Jivcov, S., Kusch, S., Munz, P., Niedermeyer, E., Osborne, A., Raddatz, J., Raeke, A.W., Reissig, S., Sebastian, U., Taniguchi, N., Venancio, I.M., Voigt, S., Wachholz, A., 2016. South American Hydrological Balance and Paleoceanography during the Late Pleistocene and Holocene (SAMBA), Cruise No. M125. March 21 – April 15, 2016 - Rio de Janeiro (Brazil) – Fortaleza (Brazil).

Bahr, A., Hoffmann, J., Schönfeld, J., Schmidt, M.W., Nürnberg, D., Batenburg, S.J., Voigt, S., 2018. Low-latitude expressions of high-latitude forcing during Heinrich stadial 1 and the younger Dryas in northern south America. Glob. Planet. Chang. 160, 1–9. https://doi.org/10.1016/j.gloplacha.2017.11.008.

Baker, P. a, Rigsby, C. a, Seltzer, G.O., Fritz, S.C., Lowenstein, T.K., Bacher, N.P., Veliz, C., 2001. Tropical climate changes at millennial and orbital timescales on the Bolivian Altiplano. Nature 409, 698–701. https://doi.org/10.1038/35055524.

Behling, H., Arz, H.W., Pätzold, J., Wefer, G., 2002. Late Quaternary vegetational and climate dynamics in southeastern Brazil, inferences from marine cores GeoB 3229-2 and GeoB 3202-1. Palaeogeogr. Palaeoclimatol. Palaeoecol. https://doi.org/10.1016/S0031-0182(01)00435-7.

Berbery, E.H., Barros, V.R., 2002. The hydrologic cycle of the La Plata basin in South America. J. Hydrometeorol. https://doi.org/10.1175/1525-7541(2002)003<0630:THCOTL>2.0.CO;2.

Blaauw, M., Christen, J.A., 2011. Flexible paleoclimate age-depth models using an autoregressive gamma process. Bayesian Anal. 6, 457–474. https://doi.org/10.1214/11-BA618.

Broccoli, A.J., Dahl, K.A., Stouffer, R.J., 2006. Response of the ITCZ to northern hemisphere cooling. Geophys. Res. Lett. 33, 1–4. https://doi.org/10.1029/2005GL024546.

Butzin, M., Köhler, P., Lohmann, G., 2017. Marine radiocarbon reservoir age simulations for the past 50,000 years. Geophys. Res. Lett. 44, 8473–8480. https://doi.org/10.1002/2017GL074688.

Campos, M.C., Chiessi, C.M., Mulitza, S., 2019. XRF Ti/Ca Ratios of Sediment Core GeoB6212-1. Campos, MC et al. (2019). PANGAEA. https://doi.org/10.1594/PANGAEA.897977. (Accessed 19 March 2019).

Carvalho, L.M.V., Jones, C., Liebmann, B., 2004. The South Atlantic convergence zone: intensity, form, persistence, and relationships with intraseasonal to interannual activity and extreme rainfall. J. Clim. 17, 88–108. https://doi.org/10.1175/1520-0442(2004)017<0088:TSACZI>2.0.CO;2.

Chaves, R.R., Nobre, P., 2004. Interactions between sea surface temperature over the south Atlantic ocean and the south Atlantic convergence zone. Geeophys. Res. Lett. 31, L03204. https://doi.org/10.1029/2003GL018647.

Collins, W.D., Bitz, C.M., Blackmon, M.L., Bonan, G.B., Bretherton, C.S., Carton, J.A., Chang, P., Doney, S.C., Hack, J.J., Henderson, T.B., Kiehl, J.T., Large, W.G., McKenna, D.S., Santer, B.D., Smith, R.D., 2006. The community climate system model version 3 (CCSM3). J. Clim. https://doi.org/10.1175/JCLI3761.1.

Cook, K.H., Vizy, E.K., 2006. South American climate during the last glacial maximum: delayed onset of the south American monsoon. J. Geophys. Res. Atmos. 111, 1–21. https://doi.org/10.1029/2005JD005980.

Crivellari, S., Chiessi, C.M., Kuhnert, H., Häggi, C., da Costa Portilho-Ramos, R., Zeng, J.Y., Zhang, Y., Schefuß, E., Mollenhauer, G., Hefter, J., Alexandre, F., Sampaio, G., Mulitza, S., 2018. Increased Amazon freshwater discharge during late Heinrich stadial 1. Quat. Sci. Rev. 181, 144–155. https://doi.org/10.1016/j.quascirev.2017.12.005.

Cruz, F.W., Burns, S.J., Jercinovic, M., Karmann, I., Sharp, W.D., Vuille, M., 2007. Evidence of rainfall variations in Southern Brazil from trace element ratios (Mg/Ca and Sr/Ca) in a Late Pleistocene stalagmite. Geochem. Cosmochim. Acta 71, 2250–2263. https://doi.org/10.1016/j.gca.2007.02.005.

Cruz, F.W., Burns, S.J., Karmann, I., Sharp, W.D., Vuille, M., Cardoso, A.O., Ferrari, J.A., Silva Dias, P.L., Viana, O., 2005. Insolation-driven changes in atmospheric circulation over the past 116,000 years in subtropical Brazil. Nature 434, 63–66. https://doi.org/10.1038/nature03365.

Cruz, F.W., Vuille, M., Burns, S.J., Wang, X., Cheng, H., Werner, M., Lawrence Edwards, R., Karmann, I., Auler, A.S., Nguyen, H., 2009. Orbitally driven east-west antiphasing of South American precipitation. Nat. Geosci. 2, 210–214. https://doi.org/10.1038/ngeo444.

Deplazes, G., Lückge, A., Peterson, L.C., Timmermann, A., Hamann, Y., Hughen, K. a, Röhl, U., Laj, C., Cane, M. a, Sigman, D.M., Haug, G.H., 2013. Links between tropical rainfall and North Atlantic climate during the last glacial period. Nat. Geosci. 6, 1–5. https://doi.org/10.1038/ngeo1712.

Dominguez, J.M.L., 1996. The São Francisco strandplain: a paradigm for wave-dominated deltas? Geol. Soc. Lond. Spec. Publ. 117, 217–231. https://doi.org/10.1144/GSL.SP.1996.117.01.13.

Duarte, C.S.L., Viana, A.R., 2007. Santos Drift system: stratigraphic organization and implications for late Cenozoic palaeocirculation in the santos basin, SW Atlantic ocean. Geol. Soc. Lond. Spec. Publ. 276, 171–198. https://doi.org/10.1144/GSL.SP.2007.276.01.09.

Erokhina, O., Rogozhina, I., Prange, M., Bakker, P., Bernales, J., Paul, A., Schulz, M., 2017. Dependence of slope lapse rate over the Greenland ice sheet on background climate. J. Glaciol. 63, 568–572. https://doi.org/10.1017/jog.2017.10.

Faugères, J.C., Stow, D.A.V., 1993. Bottom-current-controlled sedimentation: a synthesis of the contourite problem. Sediment. Geol. 82, 287–297. https://doi.org/10.1016/0037-0738(93)90127-Q.

Felis, T., Merkel, U., Asami, R., Deschamps, P., Hathorne, E.C., Kölling, M., Bard, E., Cabioch, G., Durand, N., Prange, M., Schulz, M., Cahyarini, S.Y., Pfeiffer, M., 2012. Pronounced interannual variability in tropical South Pacific temperatures during Heinrich stadial 1. Nat. Commun. https://doi.org/10.1038/ncomms1973.

Govin, A., Chiessi, C.M., Zabel, M., Sawakuchi, A.O., Heslop, D., Hörner, T., Zhang, Y., Mulitza, S., 2014. Terrigenous input off northern South America driven by

changes in Amazonian climate and the North Brazil Current retroflection during the last 250 ka. Clim. Past 10, 843–862. https://doi.org/10.5194/cp-10-843-2014.

Govin, A., Holzwarth, U., Heslop, D., Ford Keeling, L., Zabel, M., Mulitza, S., Collins, J.A., Chiessi, C.M., 2012. Distribution of major elements in Atlantic surface sediments (36°N-49°S): imprint of terrigenous input and continental weathering. Geochem. Geophys. Geosyst. 13, 1–23. https://doi.org/10.1029/2011GC003785.

Gu, F., Zonneveld, K.A.F., Chiessi, C.M., Arz, H.W., Pätzold, J., Behling, H., 2017. Long-term vegetation, climate and ocean dynamics inferred from a 73,500 years old marine sediment core (GeoB2107-3) off southern Brazil. Quat. Sci. Rev. 172, 55–71. https://doi.org/10.1016/j.quascirev.2017.06.028.

Hessler, I., Dupont, L., Bonnefille, R., Behling, H., González, C., Helmens, K.F., Hooghiemstra, H., Lebamba, J., Ledru, M.P., Lézine, A.M., Maley, J., Marret, F., Vincens, A., 2010. Millennial-scale changes in vegetation records from tropical Africa and South America during the last glacial. Quat. Sci. Rev. 29, 2882–2899. https://doi.org/10.1016/j.quascirev.2009.11.029.

Jaeschke, A., Rühlemann, C., Arz, H., Heil, G., Lohmann, G., 2007. Coupling of millennial-scale changes in sea surface temperature and precipitation off northeastern Brazil with high-latitude climate shifts during the last glacial period. Paleoceanography 22, 1–10. https://doi.org/10.1029/2006PA001391.

Kageyama, M., Merkel, U., Otto-Bliesner, B., Prange, M., Abe-Ouchi, A., Lohmann, G., Ohgaito, R., Roche, D.M., Singarayer, J., Swingedouw, D., Zhang, X., 2013. Climatic impacts of fresh water hosing under last glacial Maximum conditions: a multi-model study. Clim. Past 9, 935–953. https://doi.org/10.5194/cp-9-935-2013.

Kanner, L.C., Burns, S.J., Cheng, H., Edwards, R.L., 2012. High-latitude forcing of the south American summer monsoon during the last glacial. Science 335 (80), 570–573. https://doi.org/10.1126/science.1213397.

Knoppers, B., Ekau, W., Figueiredo, A.G., 1999. The coast and shelf of east and northeast Brazil and material transport. Geo Mar. Lett. 19, 171–178. https://doi.org/10.1007/s003670050106.

Koutavas, A., Lynch-Stieglitz, J., Marchitto, T.M., Sachs, J.P., 2002. El Niño-like pattern in ice age tropical Pacific sea surface temperature. Science 80. https://doi.org/10.1126/science.1072376.

Langner, M., Mulitza, S., 2019. Technical Note: PaleoDataView – a software toolbox for the collection, homogenization and visualization of marine proxy data. Clim. Past Discuss. 1–9. https://doi.org/10.5194/cp-2019-59.

Ledru, M.P., Ceccantini, G., Gouveia, S.E.M., López-Sáez, J.A., Pessenda, L.C.R., Ribeiro, A.S., 2006. Millenial-scale climatic and vegetation changes in a northern Cerrado (northeast, Brazil) since the last glacial maximum. Quat. Sci. Rev. 25, 1110–1126. https://doi.org/10.1016/j.quascirev.2005.10.005.

Leduc, G., Vidal, L., Cartapanis, O., Bard, E., 2009. Modes of eastern equatorial Pacific thermocline variability: implications for ENSO dynamics over the last glacial period. Paleoceanography 24, 1–14. https://doi.org/10.1029/2008PA001701.

Lentz, S.J., 1995. Seasonal variations in the horizontal structure of the Amazon Plume inferred from historical hydrographic data. J. Geophys. Res. 100, 2391. https://doi.org/10.1029/94JC01847.

Lewis, S.C., Legrande, A.N., Kelley, M., Schmidt, G.A., 2010. Water vapour source impacts on oxygen isotope variability in tropical precipitation during Heinrich events. Clim. Past 6, 325–343. https://doi.org/10.5194/cp-6-325-2010.

Lindzen, R.S., Nigam, S., 1987. On the role of sea surface temperature gradients in forcing low-level winds and convergence in the tropics. J. Atmos. Sci. 44, 2418–2436. https://doi.org/10.1175/1520-0469(1987)044<2418:OTROSS>2.0.CO;2.

Liu, Z., Lu, Z., Wen, X., Otto-Bliesner, B.L., Timmermann, A., Cobb, K.M., 2014. Evolution and forcing mechanisms of El Niño over the past 21,000 years. Nature. https://doi.org/10.1038/nature13963.

Marengo, J.A., Liebmann, B., Kousky, V.E., Filizola, N.P., Wainer, I.C., 2001. Onset and end of the rainy season in the Brazilian Amazon Basin. J. Clim. https://doi.org/10.1175/1520-0442(2001)014<0833:OAEOTR>2.0.CO;2.

Marshall, J., Donohoe, A., Ferreira, D., McGee, D., 2014. The ocean's role in setting the mean position of the Inter-Tropical Convergence Zone. Clim. Dyn. 42, 1967–1979. https://doi.org/10.1007/s00382-013-1767-z.

Merkel, U., Prange, M., Schulz, M., 2010. ENSO variability and teleconnections during glacial climates. Quat. Sci. Rev. https://doi.org/10.1016/j.quascirev.2009.11.006.

Millo, C., Strikis, N.M., Vonhof, H.B., Deininger, M., da Cruz, F.W., Wang, X., Cheng, H., Lawrence Edwards, R., 2017. Last glacial and Holocene stable isotope record of fossil dripwater from subtropical Brazil based on analysis of fluid inclusions in stalagmites. Chem. Geol. 468, 84–96. https://doi.org/10.1016/j.chemgeo.2017.08.018.

Mohtadi, M., Prange, M., Steinke, S., 2016. Review Palaeoclimatic insights into forcing and response of monsoon rainfall. Nature 533, 191–199. https://doi.org/10.1038/nature17450.

Mulitza, S., Chiessi, C.M., Schefuß, E., Lippold, J., Wichmann, D., Antz, B., Mackensen, A., Paul, A., Prange, M., Rehfeld, K., Werner, M., Bickert, T., Frank, N., Kuhnert, H., Lynch-Stieglitz, J., Portilho-Ramos, R.C., Sawakuchi, A.O., Schulz, M., Schwenk, T., Tiedemann, R., Vahlenkamp, M., Zhang, Y., 2017. Synchronous and proportional deglacial changes in Atlantic meridional overturning and northeast Brazilian precipitation. Paleoceanography 32, 622–633. https://doi.org/10.1002/2017PA003084.

Mulitza, S., Prange, M., Stuut, J.B., Zabel, M., Von Dobeneck, T., Itambi, A.C., Nizou, J., Schulz, M., Wefer, G., 2008. Sahel megadroughts triggered by glacial slowdowns of Atlantic meridional overturning. Paleoceanography. https://doi.org/10.1029/2008PA001637.

Nace, T.E., Baker, P.A., Dwyer, G.S., Silva, C.G., Rigsby, C.A., Burns, S.J., Giosan, L., Otto-bliesner, B., Liu, Z., Zhu, J., 2014. The role of North Brazil Current transport in the paleoclimate of the Brazilian Nordeste margin and paleoceanography of the western tropical Atlantic during the late Quaternary. Palaeogeogr. Palaeoclimatol. Palaeoecol. 415, 3–13. https://doi.org/10.1016/j.palaeo.2014.05.030.

Neelin, J.D., Held, I.M., 1987. Modeling tropical convergence based on the moist static energy budget. Mon. Weather Rev. 115, 3–12. https://doi.org/10.1175/1520-0493(1987)115<0003:MTCBOT>2.0.CO;2.

Oliveira, K.S.S., Quaresma, V. da S., 2017. Temporal variability in the suspended sediment load and streamflow of the Doce River. J. South Am. Earth Sci. 78, 101–115. https://doi.org/10.1016/j.jsames.2017.06.009.

Peterson, L.C., Haug, G.H., Hughen, K.A., Rohl, U., 2000. Rapid changes in the hydrologic cycle of the tropical Atlantic during the last glacial. Science (80). https://doi.org/10.1126/science.290.5498.1947.

Peterson, R.G., Stramma, L., 1991. Upper level circulation in the south Atlantic ocean. Prog. Oceanogr. 26, 1–73. https://doi.org/10.1016/0079-6611(91)90006-8.

Piola, A.R., Matano, R.P., Palma, E.D., Möller, O.O., Campos, E.J.D., 2005. The influence of the Plata River discharge on the western South Atlantic shelf. Geophys. Res. Lett. 32, 1–4. https://doi.org/10.1029/2004GL021638.

Poggemann, D.-W., Nürnberg, D., Hathorne, E.C., Frank, M., Rath, W., Reißig, S., Bahr, A., 2018. Deglacial heat uptake by the southern ocean and rapid northward redistribution via Antarctic intermediate water. Paleoceanogr. Paleoclimatol. https://doi.org/10.1029/2017PA003284.

Prange, M., Steph, S., Liu, H., Keigwin, L.D., Schulz, M., 2015. Hydroclimatic variability in the Panama bight region during termination 1 and the Holocene. In: Schulz, M., Paul, A. (Eds.), Integrated Analysis of Interglacial Climate Dynamics (INTERDYNAMIC). SpringerBriefs in Earth System Sciences, pp. 63–68.

Reimer, P.J., Bard, E., Bayliss, A., Beck, J.W., Blackwell, P.G., Ramsey, C.B., Buck, C.E., Cheng, H., Edwards, R.L., Friedrich, M., Grootes, P.M., Guilderson, T.P., Haflidason, H., Hajdas, I., Hatté, C., Heaton, T.J., Hoffmann, D.L., Hogg, A.G., Hughen, K.A., Kaiser, K.F., Kromer, B., Manning, S.W., Niu, M., Reimer, R.W., Richards, D.A., Scott, E.M., Southon, J.R., Staff, R.A., Turney, C.S.M., van der Plicht, J., 2013. IntCal13 and Marine13 radiocarbon age calibration curves 0–50,000 Years cal BP. Radiocarbon 55, 1869–1887. https://doi.org/10.2458/azu_js_rc.55.16947.

Robertson, A., Mechoso, C., 2000. Interannual and interdecadal variability of the south Atlantic convergence zone. Mon. Weather Rev. 2947–2957. https://doi.org/10.1175/1520-0493(2000)128<2947:IAIVOT>2.0.CO;2.

Schettini, C.A.F., 2002. Near bed sediment transport in the itajaí-açu river estuary, southern Brazil. In: Proceedings in Marine Science. Elsevier B.V.

Schlitzer, R., 2017. Ocean Data View. https://odv.awi.de.

Schneider, T., Bischoff, T., Haug, G.H., 2014. Migrations and dynamics of the intertropical convergence zone. Nature 513, 45–53. https://doi.org/10.1038/nature13636.

Stramma, L., England, M., 1999. On the water masses and mean circulation of the South Atlantic Ocean. J. Geophys. Res. Ocean. 104, 20863–20883. https://doi.org/10.1029/1999JC900139.

Stríkis, N.M., Chiessi, C.M., Cruz, F.W., Vuille, M., Cheng, H., De Souza Barreto, E.A., Mollenhauer, G., Kasten, S., Karmann, I., Edwards, R.L., Bernal, J.P., Sales, H.D.R., 2015. Timing and structure of mega-SACZ events during Heinrich stadial 1. Geophys. Res. Lett. 42, 5477–5484. https://doi.org/10.1002/2015GL064048.

Stríkis, N.M., Cruz, F.W., Barreto, E.A.S., Naughton, F., Vuille, M., Cheng, H., Voelker, A.H.L., Zhang, H., Karmann, I., Edwards, R.L., Auler, A.S., Santos, R.V., Sales, H.R., 2018. South American monsoon response to iceberg discharge in the North Atlantic. Proc. Natl. Acad. Sci. https://doi.org/10.1073/pnas.1717784115. U. S. A. 201717784.

Talento, S., Barreiro, M., 2017. Control of the south Atlantic convergence zone by extratropical thermal forcing. Clim. Dyn. https://doi.org/10.1007/s00382-017-3647-4.

Timmermann, A., Okumura, Y., An, S.I., Clement, A., Dong, B., Guilyardi, E., Hu, A., Jungclaus, J.H., Renold, M., Stocker, T.F., Stouffer, R.J., Sutton, R., Xie, S.P., Yin, J., 2007. The influence of a weakening of the Atlantic meridional overturning circulation on ENSO. J. Clim. 20, 4899–4919. https://doi.org/10.1175/JCLI4283.1.

Tjallingii, R., Röhl, U., Kölling, M., Bickert, T., 2007. Influence of the water content on X-ray fluorescence corescanning measurements in soft marine sediments. Geochem. Geophys. Geosyst. 8, 1–12. https://doi.org/10.1029/2006GC001393.

Venancio, I.M., Mulitza, S., Govin, A., Santos, T.P., Lessa, D.O., Albuquerque, A.L.S., Chiessi, C.M., Tiedemann, R., Vahlenkamp, M., Bickert, T., Schulz, M., 2018. Millennial- to orbital-scale responses of western equatorial Atlantic thermocline depth to changes in the trade wind system since the Last Interglacial. Paleoceanogr. Paleoclimatol. https://doi.org/10.1029/2018PA003437.

Vuille, M., Burns, S.J., Taylor, B.L., Cruz, F.W., Bird, B.W., Abbott, M.B., Kanner, L.C., Cheng, H., 2012. Of the Past A Review of the South American Monsoon History as Recorded in Stable Isotopic Proxies over the Past Two Millennia 1309–1321.

Wang, X., Auler, A.S., Edwards, R.L., Cheng, H., Cristalli, P.S., Smart, P.L., Richards, D.A., Shen, C.-C., 2004. Wet periods in northeastern Brazil over the past 210 kyr linked to distant climate anomalies. Nature 432, 740–743. https://doi.org/10.1038/nature03067.

Wang, X., Auler, A.S., Edwards, R.L., Cheng, H., Ito, E., Solheid, M., 2006. Interhemispheric anti-phasing of rainfall during the last glacial period. Quat. Sci. Rev. 25, 3391–3403. https://doi.org/10.1016/j.quascirev.2006.02.009.

Zhang, Y., Chiessi, C.M., Mulitza, S., Sawakuchi, A.O., Häggi, C., Zabel, M., Portilho-Ramos, R.C., Schefuß, E., Crivellari, S., Wefer, G., 2017. Different precipitation patterns across tropical South America during Heinrich and Dansgaard-

Oeschger stadials. Quat. Sci. Rev. 177, 1–9. https://doi.org/10.1016/j.quascirev.2017.10.012.
Zhang, Y., Chiessi, C.M., Mulitza, S., Zabel, M., Trindade, R.I.F., Hollanda, M.H.B.M., Dantas, E.L., Govin, A., Tiedemann, R., Wefer, G., 2015. Origin of increased terrigenous supply to the NE south American continental margin during Heinrich stadial 1 and the younger Dryas. Earth Planet. Sci. Lett. 432, 493–500. https://doi.org/10.1016/j.epsl.2015.09.054.
Zhang, Y., Zhang, Xu, Chiessi, C.M., Mulitza, S., Zhang, Xiao, Lohmann, G., Prange, M., Behling, H., Zabel, M., Govin, A., Sawakuchi, A.O., Cruz, F.W., Wefer, G., 2016. Equatorial Pacific forcing of western Amazonian precipitation during Heinrich stadial 1. Sci. Rep. 6, 35866. https://doi.org/10.1038/srep35866.
Zhou, J., Lau, K.M., 1998. Does a monsoon climate exist over South America? J. Clim. 11, 1020–1040. https://doi.org/10.1175/1520-0442(1998)011<1020:DAMCEO>2.0.CO;2.
Zular, A., Sawakuchi, A.O., Chiessi, C.M., d'Horta, F.M., Cruz, F.W., Demattê, J.A.M., Ribas, C.C., Hartmann, G.A., Giannini, P.C.F., Soares, E.A.A., 2019. The role of abrupt climate change in the formation of an open vegetation enclave in northern Amazonia during the late Quaternary. Glob. Planet. Chang. 172, 140–149. https://doi.org/10.1016/j.gloplacha.2018.09.006.